Advances in Science and Technology Research Journal, 2025, 19(12), 210–218 https://doi.org/10.12913/22998624/210196 ISSN 2299-8624, License CC-BY 4.0

Short-term behaviour of laminated veneer lumber slabs subjected to bending

Marcin Chybiński^{1*}, Łukasz Polus¹, Marcin Zieliński²

- ¹ Institute of Building Engineering, Faculty of Civil and Transport Engineering, Poznan University of Technology, Piotrowo 5 Str., 60-965 Poznan, Poland
- ² Graduate of the Faculty of Civil and Transport Engineering; Poznan University of Technology, Piotrowo 5 Str., 60-965 Poznan, Poland
- * Corresponding author's e-mail: marcin.chybinski@put.poznan.pl

ABSTRACT

In this paper, an investigation of the behaviour of laminated veneer lumber slabs in four-point bending tests was analysed. Two types of laminated veneer lumber (LVL) are manufactured in Poland, i.e., LVL R and LVL X. In this paper, the short-term behaviour of eight slabs made of LVL X were studied. In LVL X twenty percent of the veneers are crossbanded. In each slab, the cracking of veneer layers in the lower part of the slab in the tensile zone was observed. In two slabs, the delamination of the veneers occurred in the mid-span. Furthermore, the 3D finite element model was developed and validated against the results from the laboratory tests. In the numerical analysis, LVL X was modelled as an orthotropic material. What is more, Hill's function was used to predict the failure. The results of the simulation and from the experiments were compared, yielding similar results.

Keywords: laminated veneer lumber, timber structures, Hill's function, numerical analysis.

INTRODUCTION

Timber is a building material characterized by low density and ease of production [1]. However, defects of timber have an impact on the behaviour of timber elements. Engineering wood products have a lower number of defects than solid timber. Laminated veneer lumber (LVL) is obtained from trees using the rotary peeling method. This method makes it possible to use trees of relatively small diameters. In Poland, two types of laminated veneer lumber are produced: LVL X (with a fifth of all veneers glued crosswise) and LVL R (with all veneers glued together longitudinally) [2]. The quality of these materials is controlled during the production process. It is possible to avoid defects by carefully selecting the veneers [3]. For this reason, LVL may have better mechanical properties and less variation in these properties than solid timber. LVL has several applications in civil engineering. For example, it may be used for the construction of aircraft hangars, animal housing,

manufactories, portal frames, sports halls, swimming pools, warehouses or fertiliser sheds [4]. LVL is used for flanges of I-joists. I-joists may be combined with LVL to create a building system [5]. In this system, I-joists may be used as rafters, floor joists, wall studs, and facades, while LVL can be used in purlins, joists, beams, studs, structural panels, rim boards, headers and sole plates. New applications of this material are constantly being invented. LVL elements were used as slabs of metal-timber composite beams [6, 7] and girders of composite beams with timber or concrete slabs [8-10]. The ultimate load of LVL structural elements may be increased using carbon fabric sheets [11]. Due to its increasingly more frequent use, the behaviour of LVL should be well investigated. Furthermore, numerical models of the material should be prepared and validated. These models could be used if there is a need to analyse the behaviour of the existing or newly-designed buildings. In the paper [12], LVL R slabs subjected to bending were analysed, and the

Received: 2025.08.03

Accepted: 2025.10.01

Published: 2025.11.01

load-deflection curves were obtained. In LVL R, all veneers were glued along the grain. Furthermore, numerical models of the LVL R slabs were developed and an elastic-perfectly plastic material model and an orthotropic material model with the Hashin damage model were used. In the paper [13], 51 mm LVL-C panels with twenty percent of crossbanded veneers were analysed. The material was made of Scandinavian spruce wood. Load-deformation responses and failure modes were observed in the bending tests. However, the numerical analysis of the LVL-C panel was not conducted. In this paper, the bending behaviour of LVL X was analysed and the numerical simulation of the LVL X slab was carried out. The LVL X was made of Scots pine and Norway spruce. Its mechanical properties, such as strength and fracture behaviour, are fundamentally important. For this reason, bending tests were conducted. The mechanical properties of LVL X are essential for designing timber elements and for developing finite element models. Timber elements are not easy to model. There are many parameters to identify. The numerical model of the LVL X slab was validated thanks to the laboratory tests.

FOUR-POINT BENDING TESTS OF LVL SLABS

Eight LVL X slabs (45×200×1950 mm) were tested, in accordance with EN 408 [14]. The Instron 8505 Plus testing machine was used to apply the load and the piston speed was 5.0 mm/min. In each test, the slab deflection was measured using one linear variable differential transformer. The

ultimate load was achieved after 300 ± 120 s of the experiment. The test set-up is shown in Figure 1. The experiments were carried out to capture the behaviour of the LVL slabs, their mode of failure and load-deflection response. A spreader beam and roller supports were used to reflect the four-point bending test. Steel plates were placed between the roller supports and the LVL X panel, and between the spreader beam and the panel, to prevent the local crushing of the LVL subjected to bearing. Figure 2 presents the LVL slab in the bending test.

NUMERICAL MODEL OF THE LVL SLAB

The simulation of the LVL X slab in the four-point bending test was carried out in the Abaqus program. The numerical computations were conducted using the Newton-Raphson method. The model comprised of the slab and the steel plates. The model had two axes of symmetry. For this reason, only a quarter of the slab was prepared in the program (Figure 3). All numerical model parts were divided into eight-node cuboidal finite solid elements (C3D8R), and the maximum mesh size was 10 mm (Figure 4). The displacement was applied to the loading plates. The planes of symmetry and the fixed displacements of the model are presented in Figures 5 and 6.

The contact was modelled between the LVL slab and the steel plates (Figure 7). Surface-to-surface hard contact was applied to limit the possibility of penetration. In the laboratory tests steel plates were used to prevent the local crushing of the LVL subjected to bearing and the penetration of

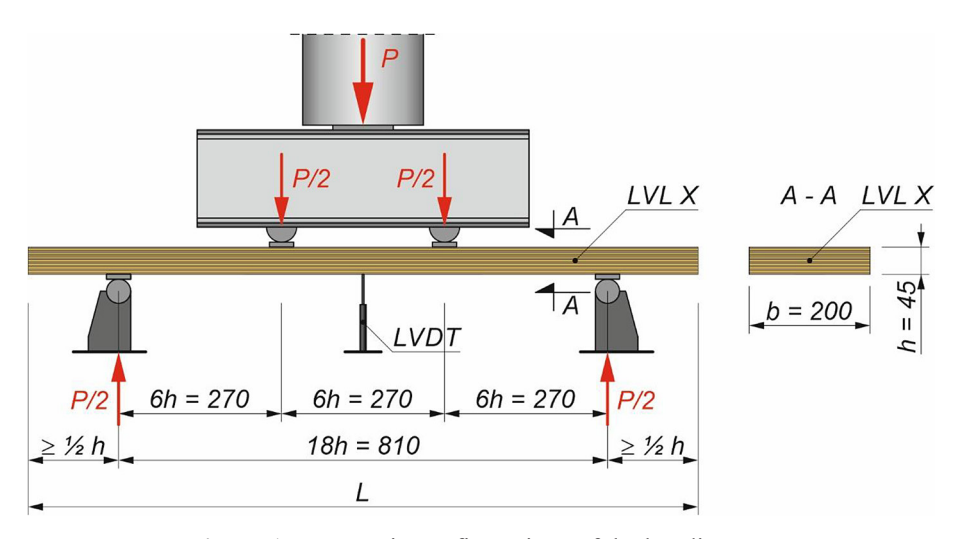


Figure 1. Geometric configurations of the bending test



Figure 2. The LVL slab in the experiment

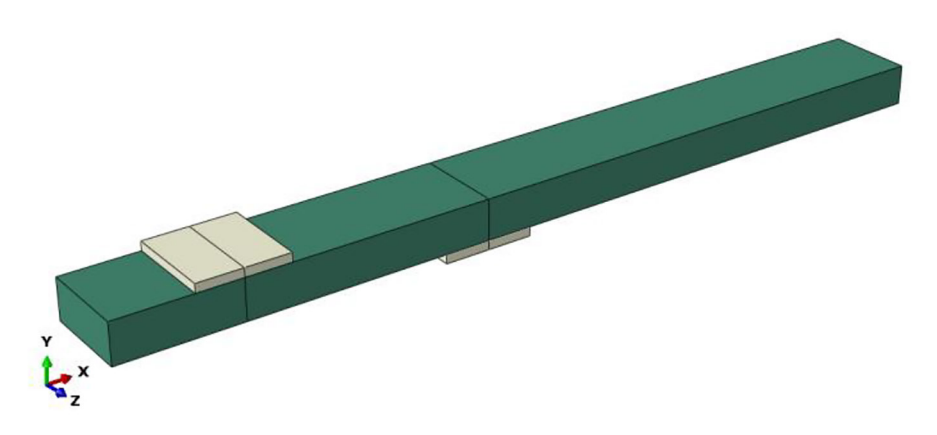


Figure 3. The LVL slab in the bending test

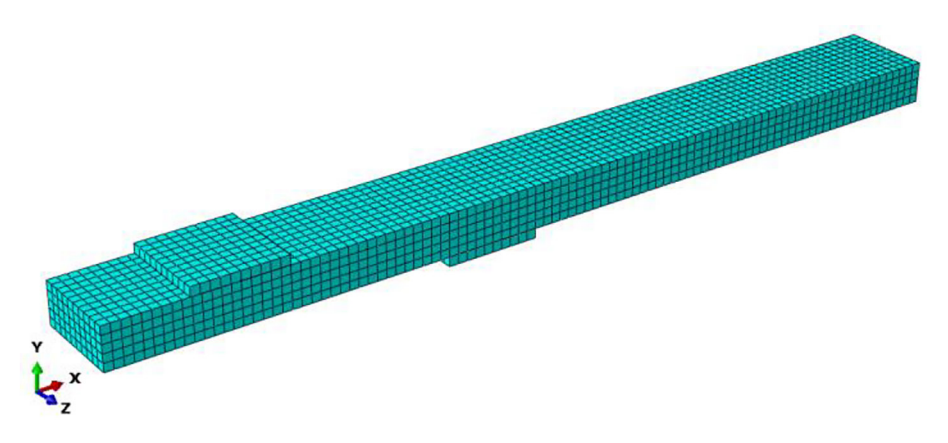


Figure 4. The mesh used in the simulation of the LVL X slab subjected to bendin

the roller elements into the LVL slab. Thanks to the steel plates, the local crushing and the penetration of the LVL were not observed in the experiments. In the case of the tangential direction, the friction coefficient equal to 0.3 was applied based on the article [15]. Dorn et al. investigated coefficients

of friction between laminated veneer lumber and steel. In the case of smooth steel surfaces, the friction coefficients ranged between 0.1–0.3.

The steel used in the plates was described as an elastic-perfectly plastic material (Poisson's ratio = 0.3, yield strength = 235 MPa, Young's

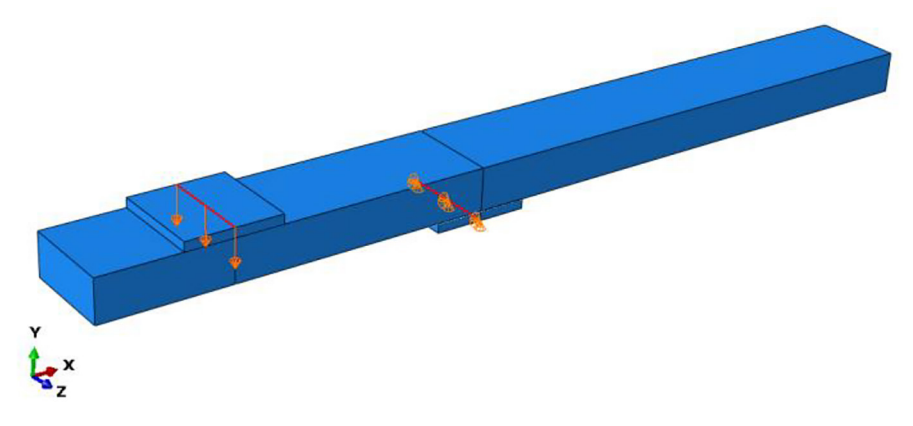


Figure 5. Displacement in y direction in the loading plate and fixed displacements in three directions in the support plate

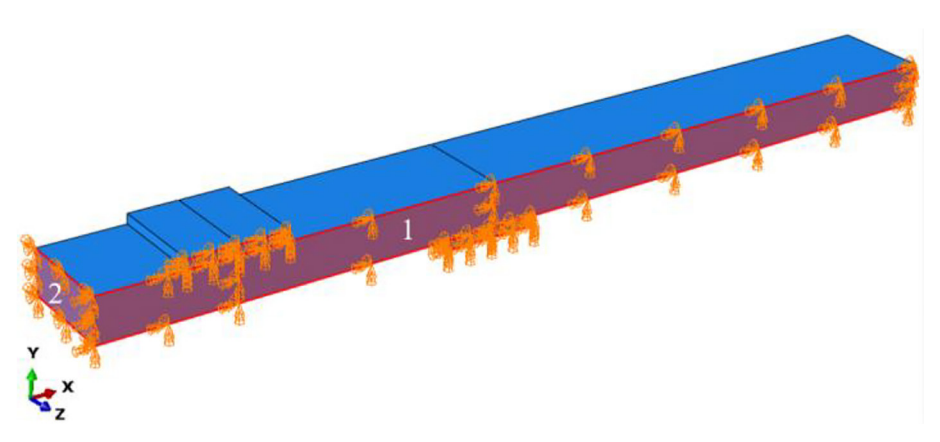


Figure 6. Two planes of symmetry: 1 - fixed displacement in the direction of z - axis and fixed rotation around two axes (x, y); <math>2 - fixed displacement in the direction of x - axis and fixed rotation around two axes (y, z)

modulus = 210 000 MPa) [16]. LVL was modelled as an orthotropic material. Furthermore, Hill's function was used to take into account the anisotropic plastic flow of the LVL after achieving its yield strength [17]. This function is a quadratic yield function with anisotropic coefficients [18, 19]. The Hill yield criterion was used in the numerical models of a wood-carbon fibre reinforced polymer joint [20] and glued laminated timber beams with reinforcing bars [21] to predict the failure. The material parameters are presented in

Table 1. Engineering constants were taken from the paper [22] to model the elastic behaviour of LVL. The calculations of Hill's function parameters are presented in Table 2. The model was divided into two equal zones, i.e., compression and tension zones. Two material models of LVL were used to distinguish between compressive and tensile strength. Similar assumption was used by Kawecki and Podgórski [17]. Hill's function parameters were calculated based on the equations presented in [23, 24]. Kawecki used the modulus

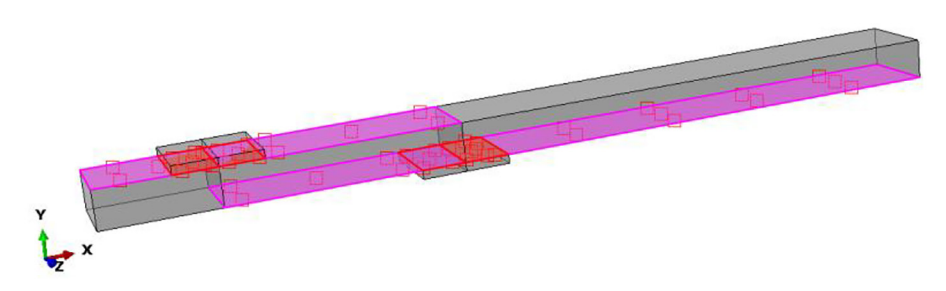


Figure 7. Contact used in the simulation of the LVL X slab subjected to bending

Table 1. Material parameters of the LVL model

Elastic behaviour (orthotropic material, engineering constants) [22]									
Elastic Modulus [MPa]			Poisson's Ratio [–]			Shear Modulus [MPa]			
E,	E ₂	E ₃	U ₁₂	U ₁₃	U ₂₃	G ₁₂	G ₁₃	G ₂₃	
13 400	700	700	0.48	0.48	0.22	900	900	90	
Tensile behaviour									
Plastic behaviour [12]		Hill's function (potential)							
Yield stress [MPa]		Plastic strain [–]	R11	R22	R33	R12	R13	R23	
41.9		0.0	0.80	0.095	0.095	0.190	0.190	0.190	
	Compressive behaviour								
Plastic behaviour [12]		Hill's function (potential)							
Yield stress [MPa]		Plastic strain [–]	R11	R22	R33	R12	R13	R23	
50).3	0.0	1.00	0.080	0.080	0.158	0.158	0.158	

Table 2. Calculations of Hill's function parameters

f _{t,1} [MPa]	f _{c,1} [MPa]	f _{c,2} [MPa]	f _{v,12} [MPa]					
41.9 [12]	50.3 [12]	4.0 [25]	4.6 [25]					
Tensile behaviour								
Para	meter	Equations [23, 24]	Value					
R	11	$R_{11} = 0.8 \frac{f_{t,1}}{f_{t,1}}$	$R_{11} = 0.8 \frac{41.9}{41.9} = 0.8$					
R22	, R33	$R_{22} = R_{33} = \frac{f_{c,2}}{f_{t,1}}$	$R_{22} = R_{33} = \frac{4.0}{41.9} = 0.095$					
R12, R	13, R23	$R_{12} = R_{13} = R_{23} = \frac{\sqrt{3 \cdot f_{v,12}}}{f_{t,1}}$	$R_{12} = R_{13} = R_{23} = \frac{\sqrt{3 \cdot 4.6}}{41.9} = 0.190$					
	Compressive behaviour							
Para	meter	Equations [23, 24]	Value					
R	11	$R_{11} = \frac{f_{c,1}}{f_{c,1}}$	$R_{11} = \frac{50.3}{50.3} = 1.0$					
R22	, R33	$R_{22} = R_{33} = \frac{f_{c,2}}{f_{c,1}}$	$R_{22} = R_{33} = \frac{4.0}{50.3} = 0.080$					
R12, R	13, R23	$R_{12} = R_{13} = R_{23} = \frac{\sqrt{3 \cdot f_{v,12}}}{f_{c,1}}$	$R_{12} = R_{13} = R_{23} = \frac{\sqrt{3 \cdot 4.6}}{50.3} = 0.158$					

of rupture (tensile strength from the bending tests) as the reference value [24]. In this paper, the reference values for the coefficients used in the compression and in the tension were the compressive strength (f_{tl}) and the tensile strength (f_{tl}) , respectively. The compressive and tensile strength (f_{cl}) and f_{tl} were taken from the laboratory tests presented in [12] and the compressive and shear strength (f_{c2}) and $f_{v,l2}$ were based on the values declared by the manufacturer in [25]. In the case of the R11 parameter for the tension region, the parameter equal to 0.8 was used. The same value of

this parameter was used by Kawecki to calibrate the strength in the tension region [24].

RESULTS

The failure mode of the LVL slabs (cracking of veneers and delamination in the lower part of the slab in the tensile zone) is presented in Figure 8. Figures 9 and 10 show the load-deflection relationships from the experiments and the numerical simulation.



Figure 8. Failure modes of the LVL slabs

The vertical displacement increased linearly up to the ultimate load. Then, a load drop caused by the veneer failure was observed. Failure modes were observed in the tensioned parts of the slabs because the tensile strength of LVL X is lower than the compressive one. The cracking of the edge veneer occurred in the tested slabs. In slab S3, the shearing of the veneers was observed under one of the forces, while delamination of the veneers occurred in the mid-span.

Delamination of veneers was also observed in slab S5. The load-bearing capacity of slab S2 was the lowest. The edge veneer connection was near the mid-span in this slab. The maximum load P_{max} , the bending resistance M, and the mid-span deflection corresponding to the maximum load $u(P_{max})$ are presented in Table 3. The bending resistance from the numerical simulation (3.88 kNm) was 4% lower than the mean value from the laboratory tests (4.04 kNm).

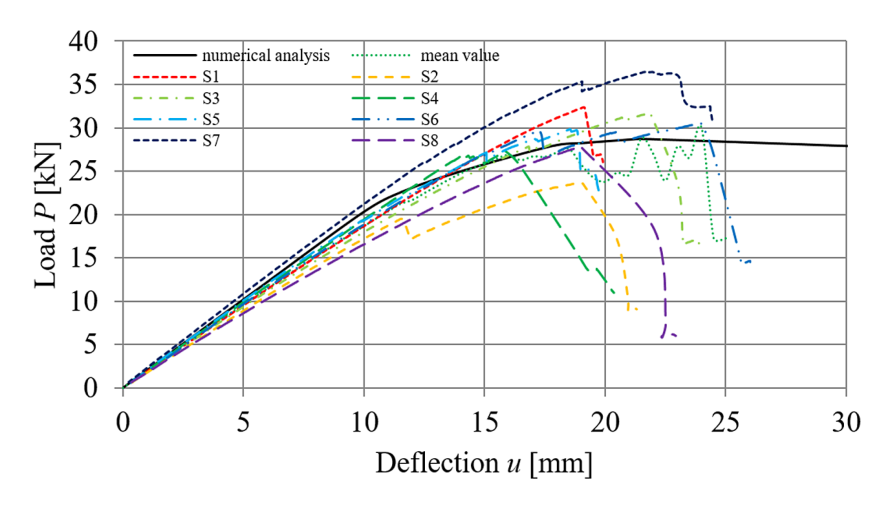


Figure 9. Load-deflection relationships from the laboratory tests and the numerical simulation

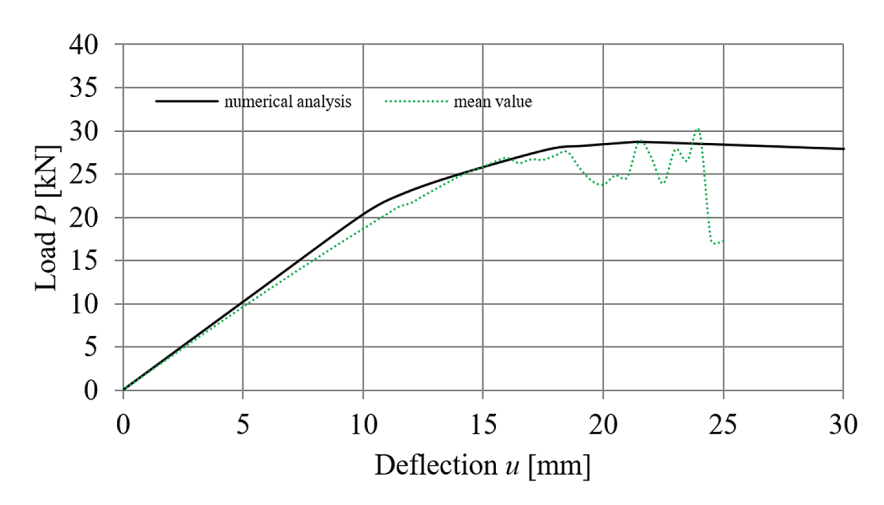


Figure 10. Comparison of the load-deflection relationships from the experiments and the numerical simulation

Table 3. Results of laboratory tests and numerical simulation

Sample	P _{max} [kN]	u(P _{max}) [mm]	<i>M</i> [kNm]	
1	32.37	19.12	4.37	
2	23.60	18.84	3.19	
3	31.74	21.87	4.28	
4	27.28	15.88	3.68	
5	29.85	18.54	4.03	
6	30.48	23.99	4.11	
7	36.47	21.69	4.92	
8	27.83	18.99	3.76	
Mean value (m)	29.95	19.86	4.04	
Numerical (n)	28.71	21.35	3.88	
n/m	0.96	1.08	0.96	

In the numerical simulation, the ultimate load was achieved when the strength of LVL X was achieved both at the bottom and upper parts of the LVL X slab (Figure 11). The area of the tension zone in which tensile strength was achieved was larger than the area of the compression zone in

which compressive strength was achieved. Tensile strength was achieved over the entire height of the tension zone. In the laboratory tests, failure modes were observed in the tensioned parts of the slabs. The numerical model captured the response of the LVL X slab relatively well.

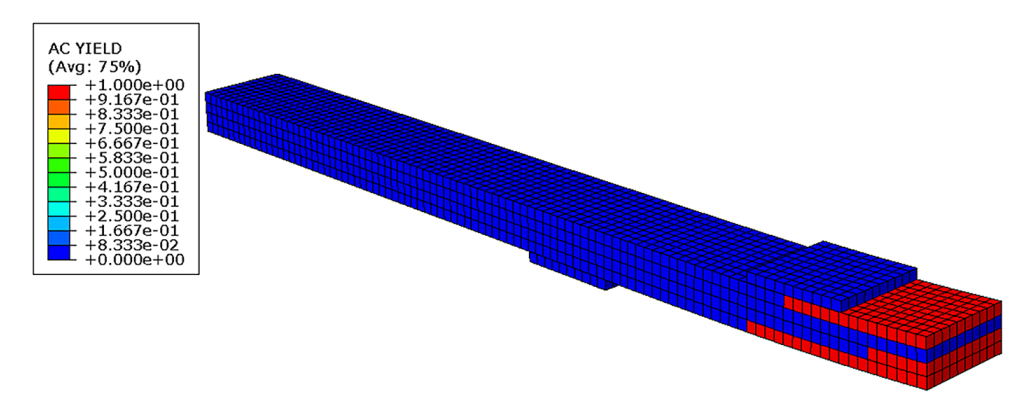


Figure 11. Failure mode in the numerical simulation for M = 4.1 kNm (a quarter of the model)

COCLUSIONS

This paper investigated the eight LVL X slabs in four-point bending tests, capturing their failure behaviour. The slabs were damaged due to the cracking of veneers in the tensile zone. In two slabs the delamination of veneers was also observed. A numerical model of the LVL slab was developed and LVL X was modelled taking into account its orthotropy. Hill's function was used to predict the failure. The results from the numerical analysis were similar to the results from the experiments. The maximum load from the numerical simulation was 4% lower than the mean value from the laboratory tests. The material model of LVL X analysed in this paper may be used in future simulations of LVL X panels and beams, and in composite beams with LVL X slabs subjected to static bending loads.

The experimental study presented in this article had certain limitations. Only the short-term behaviour of LVL X slabs subjected to bending were studied. Long-term behaviour of LVL X slabs and the influence of the moisture content of LVL X on the load-bearing capacity should be analysed in the future.

REFERENCES

- Wdowiak-Postulak A., Świt G., Dziedzic-Jagocka I. Application of Composite Bars in Wooden. Full-Scale, Innovative Engineering Products-Experimental and Numerical Study. Materials 2024; 17(3): 730. https://doi.org/10.3390/ma17030730.
- Komorowski M., Podręcznik projektowania i budowania w systemie STEICO. Podstawy. Fizyka budowli. Zalecenia wykonawcze, Forestor Communication: Warszawa 2020.

- Castanié B., Peignon A., Marc C., Eyma F., Cantarel A., Serra J., Curti R., Hadiji H., Denaud L., Girardon S., Marcon B. Wood and plywood as eco-materials for sustainable mobility: A review. Composite Structures 2024; 329: 117790. https://doi.org/10.1016/j.compstruct.2023.117790.
- 4. The LVL kitset portal frame solution, hyFRAME LVL Kitset Brochure, Carter Holt Harvey Woodproducts, 2018.
- 5. Technical Guide, STEICO construction, 2021.
- Chybiński M., Polus Ł. Experimental and numerical investigations of aluminium-timber composite beams with bolted connections. Structures 2021; 34: 1942–1960. https://doi.org/10.1016/j.istruc.2021.08.111.
- Hassanieh A., Valipour H.R., Bradford M.A., Experimental and numerical study of steel-timber composite (STC) beams. Journal of Constructional Steel Research 2016; 122: 367–378. https://doi.org/10.1016/j.jcsr.2016.04.005.
- 8. Chiniforush A.A., Valipour H.R., Ataei A. Timber-timber composite (TTC) connections and beams: An experimental and numerical study. Construction and Building Materials 2021; 303: 124493. https://doi.org/10.1016/j.conbuildmat.2021.124493.
- Khorsandnia N., Valipour H.R., Crews K. Experimental and analytical investigation of short-term behaviour of LVL-concrete composite connections and beams. Construction and Building Materials 2012; 37: 229–238. https://doi.org/10.1016/j.conbuildmat.2012.07.022.
- Yeoh D., Fragiacomo M., Deam B.. Experimental behaviour of LVL-concrete composite floor beams at strength limit state. Engineering Structures 2011; 33(9): 2697–2707. https://doi.org/10.1016/j. engstruct.2011.05.021.
- Bakalarz M., Kossakowski P. Mechanical properties of laminated veneer lumber beams strengthened with CFRP sheets. Archives of Civil Engineering 2019; 65(2): 57–66. https://doi.org/10.2478/ace-2019-0018.

- Chybiński M, Polus Ł. Experimental and numerical investigations of laminated veneer lumber panels.
 Archives of Civil Engineering 2021; 67(3): 351–372. https://doi.org/10.24425/ace.2021.138060.
- Romero A., Odenbreit C. Experimental Investigation on Strength and Stiffness Properties of Laminated Veneer Lumber (LVL). Materials 2023; 16: 7194. https://doi.org/10.3390/ma16227194.
- 14. EN 408, Timber structures Structural timber and glued laminated timber Determination of some physical and mechanical properties; European Committee for Standardization: Brussels, Belgium, 2012.
- 15. Dorn M, Habrová K, Koubek R, Serrano E., Determination of coefficients of friction for laminated veneer lumber on steel under high pressure loads. Friction 2020; 9: 367–379.
- 16. EN 1993-1-1, Design of Steel Structures, General rules and rules for buildings, European Committee for Standardization: Brussels, Belgium, 2006.
- 17. Kawecki B., Podgórski J. 3D Abaqus Simulation of Bent Softwood Elements. Archives of Civil Engineering 2020; 66(3): 323–337. https://doi.org/10.24425/ace.2020.134400.
- Cardoso R.P.R., Adetoro O.B. A generalisation of the Hill's quadratic yield function for planar plastic anisotropy to consider loading direction. International Journal of Mechanical Sciences 2017; 128–129: 253–268. https://doi.org/10.1016/j.ijmecsci.2017.04.024.

- 19. Różyło P. Stateczność i stany graniczne ściskanych cienkościennych profili kompozytowych, Wydawnictwo Politechniki Lubelskiej: Lublin, 2019.
- 20. Kawecki B. Numerical Modelling and Experimental Testing on Polyurethane Adhesively Bonded Joints Behaviour in Wood-Wood and Wood-Carbon Fibre Reinforced Polymer Layouts. Advances in Science and Technology Research Journal 2023; 17(2): 36–52. https://doi.org/10.12913/22998624/159723.
- 21. Wdowiak-Postulak A., Kawecki B. Investigations on structural-sized GLT beams reinforced with steel and FRP composite bars: experimental tests and nonlinear numerical approach. Archives of Civil and Mechanical Engineering 2025; 25, 80. https://doi.org/10.1007/s43452-025-01123-8.
- Abramowicz M., Chybiński M., Polus Ł., Wróblewski T. Free Vibrations of Sustainable Laminated Veneer Lumber Slabs. Sustainability 2024; 16(1): 166. https://doi.org/10.3390/su16010166.
- 23. Abaqus Documentation.
- 24. Kawecki B. Dobór parametrów modeli obliczeniowych pełnych dźwigarów z kompozytów drewnopolimerowych zbrojonych włóknami, Wydawnictwo Politechniki Lubelskiej: Lublin, 2021.
- 25. Declaration of performance No. 03-0006-03, STEICO LVL X.